**EML-603**

# Fluence Evaluations For Applications of *In Situ* Gamma-Ray Spectrometry in Non-Flat Terrain

**Kevin M. Miller**

**Environmental Measurements Laboratory**
**U.S. Department of Energy**
**201 Varick Street, 5th Floor**
**New York, NY 10014-4811**

**February 1999**

## DISCLAIMER

# ABSTRACT

Evaluations of gamma-ray fluence are made for source geometries that depart from the flat ground geometry that is used in standard applications of *in situ* spectrometry. Geometries considered include uniform source distributions for soil mounds on top of flat terrain, cylindrical wells, and rectangular trenches. The results indicate that scaling the standard fluence values for flat terrain by the ratio of solid angle subtended by the soil to $2\pi$ leads to fluence estimates that are accurate to within a few percent. Practical applications of *in situ* spectrometry in non-flat terrain also appears to be simplified by the fact that the angular correction factor for a typical co-axial detector in these geometries may typically be about the same as that computed for flat ground.

# TABLE OF CONTENTS

# INTRODUCTION

*In situ* gamma-ray spectrometry is commonly used to measure radionuclide concentrations, deposition, and associated dose rates in the outdoor environment (Beck et al. 1972; ICRU 1994). Measurements performed over flat ground allow for the source geometry to be represented as an infinite half-space, i.e., a $2\pi$ geometry in terms of the solid angle subtended by the source. *In situ* spectrometry has also been applied on a more limited basis for indoor measurements (Miller and Beck 1984; Miller et al. 1997). In this situation, the source geometry can sometimes be approximated as $4\pi$, depending upon the uniformity of the surrounding source distribution.

A practical need has arisen in recent years for applications of *in situ* spectrometry to support the vast environmental remediation efforts within the Department of Energy. In many situations, measurements of radionuclide concentrations will have to be made in complex terrain, i.e., soil that cannot be approximated as flat ground. For large departures from flat ground such as below-grade measurements, the fluence per unit source concentration would be expected to vary considerably from that calculated for a $2\pi$ source geometry.

This report examines the effects of varying the source geometry from that of flat ground. Included are calculations of uncollided fluence (hereafter in this report termed simply as fluence) for soil mounds on top of flat ground as well as depressions, namely, cylindrical wells (ditches) and rectangular trenches of various dimensions. Comparisons to simple solid angle calculations are made and conclusions are drawn which should tend to simplify the application of the technique in non-flat terrain. The implications with respect to practical applications of *in situ* spectrometry for such geometries and detector angular response are also examined.

# CALCULATIONS

## BASIC CONSIDERATIONS

A common method of determining the radionuclide concentration is to take and analyze a 15 cm deep soil sample. After processing, this sample provides an average over that depth, regardless of the actual profile in that soil cut. Instead of a straight average such as this, an *in situ*

spectrometric measurement provides an average that is weighted towards the surface soil where the weighting will vary according to the energy of the gamma ray. Depending upon soil density, the effective averaging depth for an energy such as 100 keV is over the first few cm, while for an energy such as 1000 keV, it is on the order of 10 cm. The viewing depth is greatest directly under a detector and it grows more shallow as the radius outward increases. The overall soil volume that is measured is thus shaped like a plano-convex lens.

Early on in the development *in situ* spectrometry, ground roughness was recognized as an important factor that could effect the fluence reaching a detector from source distributions that were on or near the soil surface (Beck et al. 1972). Even for freshly deposited fallout, a plane source would tend to over-predict the fluence due to small undulations in the soil which would essentially obstruct a direct line of sight to the source and thus provide shielding.

In environmental remediation work, however, most realistic source distributions will tend to be deeply distributed and, in effect, best approximated by a uniform profile. Using a uniform source profile as default is in keeping with cleanup criteria which tend to be dose-based and specified as a uniform concentration in surface soil.

Approximating the source distribution as uniform and converting measured count rates to concentrations virtually eliminates concerns over small perturbations in the terrain. A recent study (Laedermann et al. 1998), has shown that ground roughness, as approximated with bumps up to 20 cm in height in the terrain, is not an important factor for a measurement at 1 m above the ground of sources that are distributed in the soil. As will be brought out in the following sections, this is understandable from simple solid angle considerations and the fact that air attenuation is a secondary effect for close distances to the source interface.

## FLUENCE BASED ON SOLID ANGLE

### Infinite Media

Equations to yield the fluence for a variety of standard source geometries can be found in (USAEC 1956). Using a uniform source model allows for straightforward calculations of fluence. The case of fluence within a cavity is considered first. If a single medium (which we take to be soil or soil-like) is more than several mean free paths thick, it can be considered infinite in thickness for photon transport. For 100 keV and 1000 keV, the mean free paths in typical soil at

a density of 1.6 g $cm^{-3}$ are about 4 and 10 cm, respectively. Neglecting the effects of air attenuation, the fluence at a measurement point is simply a function of the solid angle subtended by the surrounding soil and its attenuation properties. Thus, within a cavity (full $4\pi$ geometry) with a photon mass absorption coefficient $\mu_\rho$ ($cm^2$ $g^{-1}$), density $\rho$ (g $cm^{-3}$) and a photon emission per unit volume $S_0$ ($cm^{-3}$), the fluence ($cm^{-2}$) is simply

$$\Phi = \frac{S_0}{m_r r} \tag{1}$$

Infinite Half-Space Geometry

For a measurement point above flat ground ($2\pi$ geometry or half-space), the fluence would be just one half that given by Equation 1, again neglecting the effects of air attenuation. In reality, the actual fluence would be somewhat less due to the presence of air and would therefore depend upon the energy of the photon and the height above the ground.

Figure 1 shows the theoretical fluence per unit source strength (1 photon per gram) as a function of energy for a flat ground geometry based on this simple solid angle model using values of $\mu_\rho$ given for typical soil at a 10% moisture content and a density of 1.6 g $cm^{-3}$. Also shown in this figure are the results of calculations for a point 1 m above the ground using this same soil mix and taking into consideration the air attenuation effect (Beck et al. 1972). Despite neglecting the air attenuation effect, the solid angle calculation overestimates the actual fluence by only about 11% at 50 keV. This percentage overestimate gradually reduces to about 2% at 2500 keV. Thus, the simple solid angle model gives fair results for a detector that is not too far (on the order of a meter) from the source interface.

Solid Angle Generalization

Other source geometries besides flat ground can be considered in terms of their solid angle. The differential solid angle in a polar coordinate system, as depicted in Figure 2, is expressed as

$$d\Omega = \sin\theta' \, d\theta' \, d\phi \tag{2}$$

Integration can then be performed over the volume of interest to give the total solid angle subtended.

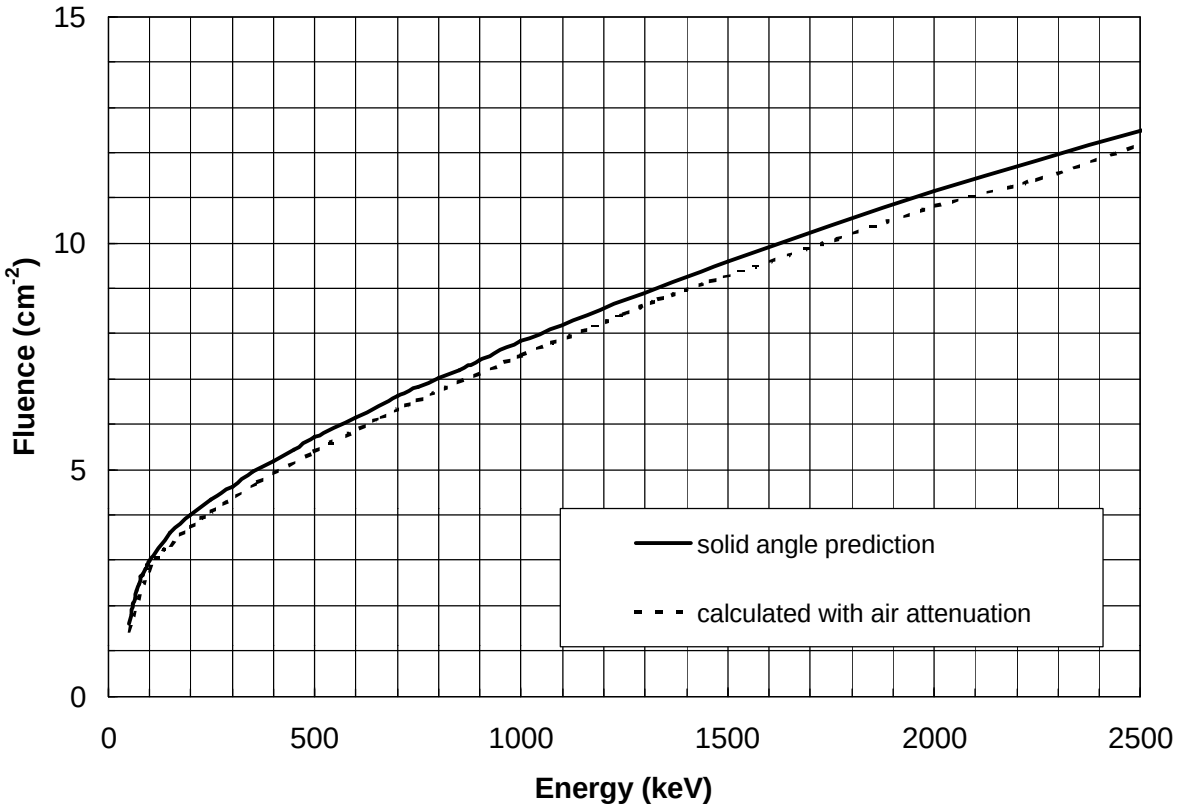


**Figure 1.** Fluence as a function of energy at 1 m above flat ground with a uniform source distribution with depth and a source emission of 1 photon per gram of soil.

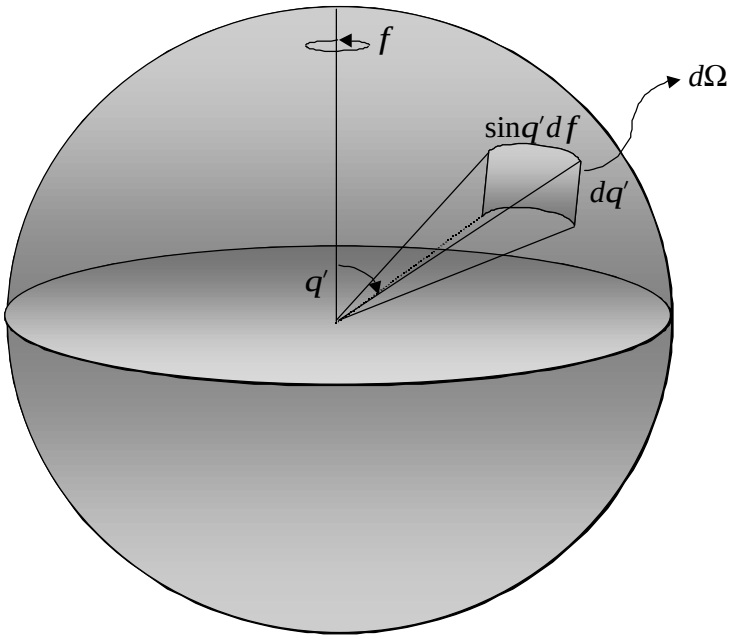


**Figure 2.** Differential solid angle element in polar coordinate system.

Soil Mounds

The case of one or more soil mounds on top of an otherwise flat terrain presents no change to the solid angle if the mounds lie below the horizontal plane of the detector. Thus, for a detector that is 1 m above the ground, mounds of up to 1 m in height would only modify the fluence at the measurement point from changes in the air path length and resultant attenuation. For each meter of air, attenuation amounts to only 1.8% at 100 keV and 0.8% at 1000 keV.

The presence of mounds does change the particular soil volume being measured. The near side of a thick mound is essentially viewed by the detector, and the volume of soil on the far side of the mound, as well as the area of ground that is shadowed behind the mound, does not contribute to the measured fluence. This type of shadowing effect is depicted in Figure 3.

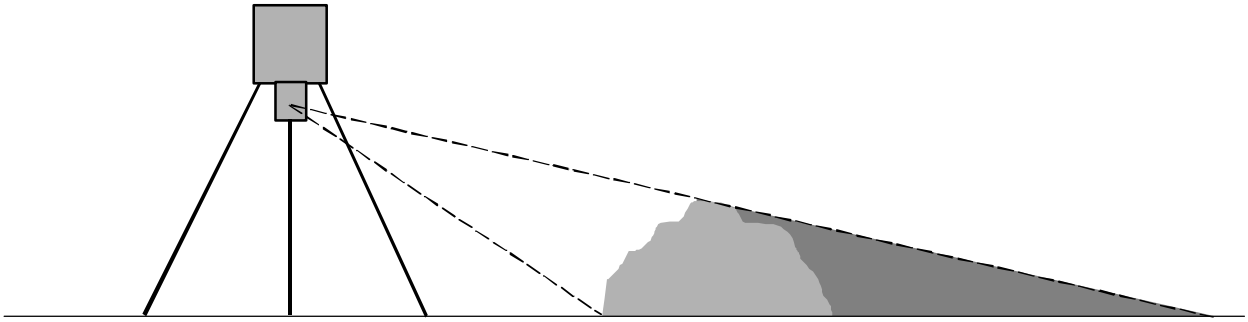

**Figure 3.** Shadowing effect produced by the presence of a soil mound atop flat terrain within the field of view of a detector.

Placing a mound directly under a detector also does not change the solid angle from $2\pi$ if the mound is finite in size and superimposed over flat terrain. A change in the solid angle would only occur for a measurement point at the apex of a hilltop (as approximated by a cone) where the ground slopes downward to infinity in all directions, which in practical applications, is not realistic.

Well Geometry

In the case of a cylindrical well (Figure 4), we note the point P at some height *h* above the floor of the well at a radial distance *X* to the wall of height *H*.

The solid angle missing from the soil source geometry (the open sky area overhead) is given by

$$\Omega' = \int_0^{2p} \int_0^{q_c'} \sin q' \, dq' \, df \tag{3}$$

which yields

$$\Omega' = 2p \, (1 - \cos q_c') \tag{4}$$

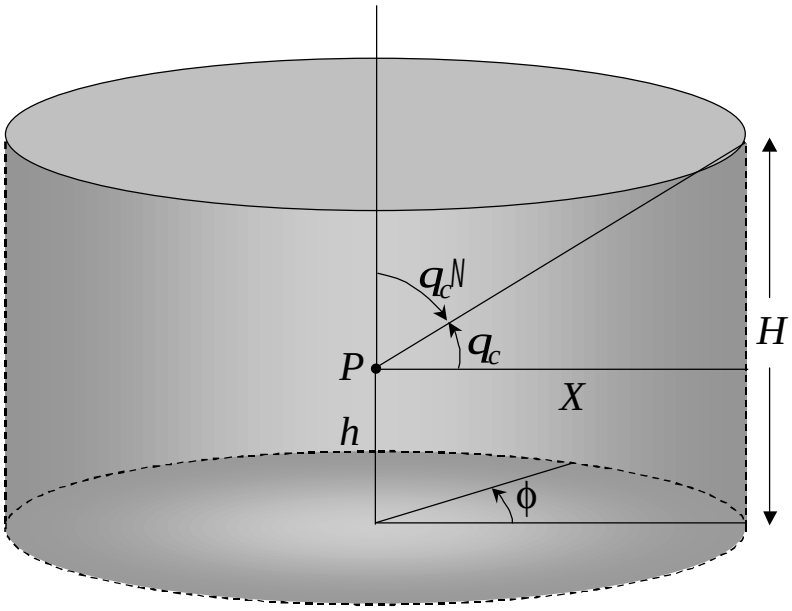


**Figure 4.** Cylindrical well geometry.

The solid angle subtended by the soil, Ω, is 4π minus this quantity and since cos$2'$ = sin$2$, where $2$ is the complement of $2'$, we have

$$\Omega = 2p \, (1 + \sin q_c) \tag{5}$$

The critical angle $\theta_c$ (henceforth called the horizon angle, i.e., the angle measured from the horizontal to the point of soil-air interface at the top of the well) can be related to the well dimensions as

$$q_c = \tan^{-1}\left(\frac{H-h}{X}\right) \tag{6}$$

Trench Geometry

For the case of an infinitely long trench, we refer to Figure 5 where we note the point *P* is in the middle of the trench at some height *h* above the trench floor and a wall height *H*. The distance to the wall is denoted as *X* which is the trench half-width.

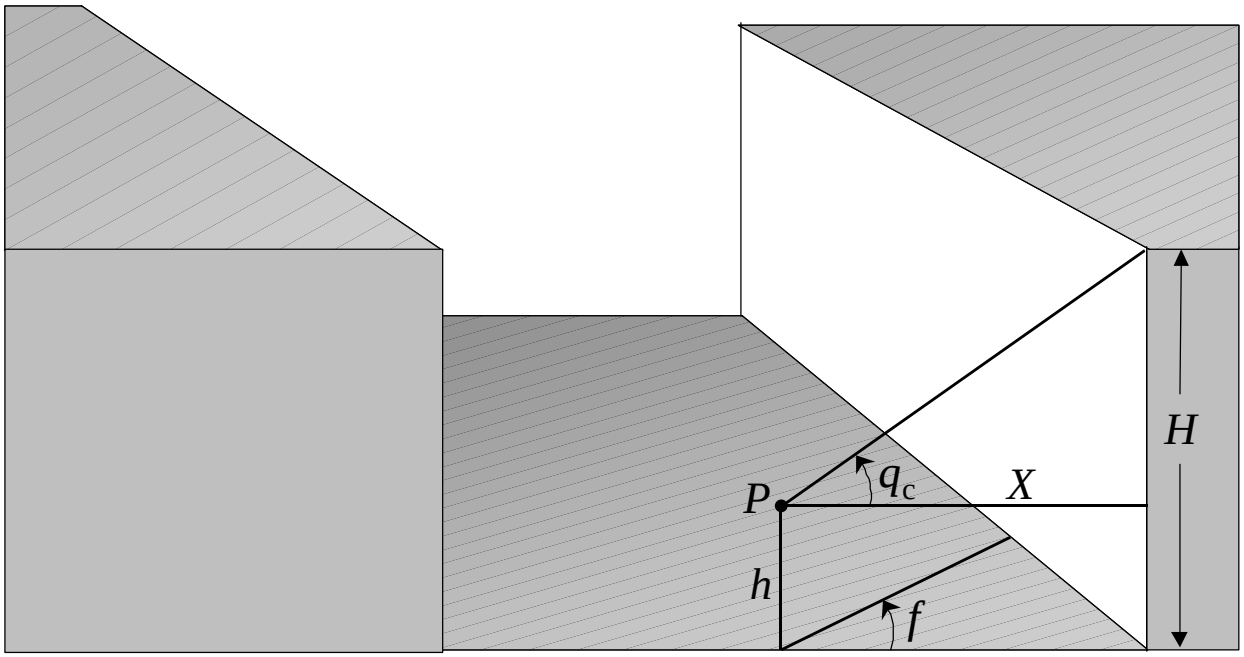


**Figure 5.** Generalized vertical wall trench geometry.

Using the previous result, the solid angle subtended by the soil volume in the half space above point P would be

$$\Omega = \int_0^{2p} \sin\left[q_c(f)\right] df \tag{7}$$

where $2_c$ is seen to be a function of $N$, that is,

$$q_c = \tan^{-1}\left[\frac{(H-h)\cos f}{X}\right] \tag{8}$$

Using symmetry we can break the computation into four equal quadrants and the total solid angle of soil subtended in the center of the trench would be

$$\Omega = 4\int_0^{p/2} \sin\left\{\tan^{-1}\left[\frac{(H-h)\cos f}{X}\right]\right\} df \tag{9}$$

which yields

$$\Omega = 4\tan^{-1}\left(\frac{H-h}{X}\right) = 4q_{c0} \tag{10}$$

where $2_{c0}$ is the horizon angle at $N = 0$. The volume of soil below point $P$ represents a half-space or $2\pi$ contribution so the total solid angle for the trench geometry would then be

$$\Omega_t = 2p + 4q_{c0} \tag{11}$$

Apart from neglecting air attenuation, an additional source of overestimation using a simple solid angle model occurs from treating the soil at the top edge of the well or trench as infinitely thick. In fact, the photon path length through the soil tends to be less than several mean free paths at the top edge, although the fraction of the total soil volume where this holds true is rather

small. With this in mind, a reasonable upper bound to the fluence can, therefore, be calculated using Equation 1 and scaling the result by the fraction of the full $4\pi$ solid angle given by either Equations 6 or 11, i.e., the ratio $\Omega/4\pi$. The results of these solid angle calculations will be subsequently used as a basis of comparison to calculations that take into account the air attenuation effect.

## FLUENCE WITH AIR ATTENUATION EFFECT

To calculate the fluence for the source geometries investigated in this report, a point kernel numerical integration method was applied. Alternative methods include analytical solutions using series expansion or Monte Carlo methods. However, numerical integration methods are straightforward to set up, flexible in adjusting source terms within the geometry, and, given the processing speed of current desktop computers, not unduly slow to perform.

In general, the total fluence ($cm^{-2}$) for a point P that is not close to the source, i.e., tens of cm or more (Figure 6), is the summation of the contribution from all volume elements of source strength, $S_i$ (photons per $cm^3$), with dimensions $\Delta x\, \Delta y\, \Delta z$ within some volume, $V$

$$\Phi = \sum_i \frac{e^{-\mu_{r_a} r_a r_a}\, e^{-\mu_{r_s} r_s r_s} S_i \Delta x \Delta y \Delta z}{4p\ r^2} \tag{12}$$

where $r$ (cm) is the distance the photon traverses, that is, $r_a + r_s$ or $\sqrt{(x^2+y^2+z^2)}$ and the subscripts $a$ and $s$ denote the respective air and soil values for the mass absorption coefficient, density, and distance.

Given the scale of the detector/source geometry and the absorption properties of soil, a volume element 1 $cm^3$ in size was used to perform the calculations. This is considered sufficiently small to achieve adequate accuracy for the source/detector geometries used in this study. As a justification, note that the self attenuation for parallel fluence through a volume of thickness, $t$, with a uniform source concentration is given by the expression

$$\frac{I}{I_0} = \frac{1 - e^{-\mu_r r t}}{\mu_r r t} \tag{13}$$

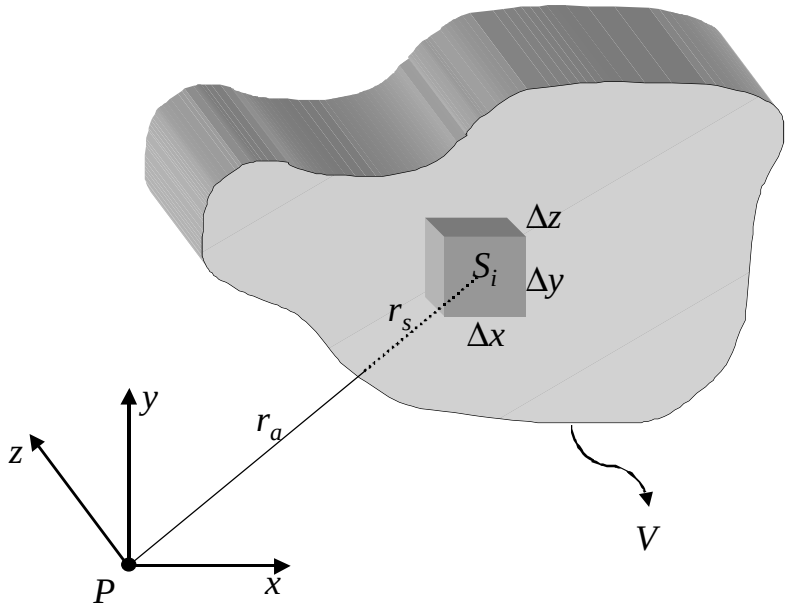


**Figure 6.** Soil volume element for arbitrary geometry in rectilinear coordinate system.

For a density of 1.6 g cm$^{-3}$ and $x$ = 1 cm, this gives an attenuation value of 0.878 at 100 keV and 0.951 at 1000 keV.

Alternatively, using the center point of the volume, the self attenuation can be approximated by

$$\frac{I}{I_0} \approx e^{-m_r r t/2} \tag{14}$$

which for 100 and 1000 keV yields respective attenuation values of 0.875 and 0.950. These compare quite favorably to the exact values computed with Equation 13.

For low energies and large radial distances (>10 m), the use of a 1 cm$^3$ size volume element begins to lead to a noticeable underestimate in the fluence due to the large diagonal path through the soil volume element. An evaluation of the sensitivity to volume element size indicated that the use of 1 cm$^3$ led to convergence in the integrated fluence for finite geometries, while

maintaining an accuracy in the total fluence of better than 1% at high energies (1000 keV), and not worse than 2% at low energies (100 keV) for the trench and well dimensions used in this study. This was based on comparisons of this integration method to that of analytic solutions for a flat ground geometry.

The limits of integration were chosen to be 100 cm for depth into the ground or trench/well wall. In the case of the trench calculation, the limit in the z direction was 30 m. These limits are sufficient to account for essentially 100% of the fluence. Several different BASIC codes were written using double precision (16 digits) to perform the calculations for the different geometries. These are listed in Appendix A.

Soil Mounds

A few calculations were carried out to verify the insensitivity of the fluence to mounds less than the detector height. For example, the effect of a single mound, 50 cm high and 1 m wide extending half way around a detector at 1 m above the ground (a crescent shaped mound) would only result in a fluence increase of less than a half percent at 1 MeV. A similar shaped mound of the same thickness at a height of 1 m would lead to about a 2% increase. In the limit, the thickness, size, and number of mounds encircling a detector in effect leads to a well geometry, the results of which are given in the next section.

The situation of a mound under a detector would also produce minor effects. In the limit, for an infinitesimally narrow mound of some height, h′, the fluence would be reduced to that for a detector at a height of h + h′ above the ground. The reduction would reflect the increase in the air attenuation and would amount to about 6% at 100 keV and 3% at 1000 keV for h′ = 1 m. Any finite size mound of this height under the detector would thus produce even less of an effect.

Well Geometry

The case of the cylindrical well represents a geometry that reduces to two dimensions due to symmetry about the angle $\phi$ (Figure 7). The summation can thus be performed over rings of soil having circumference $2\pi x$. Equation 11 can then be rewritten as

$$\Phi = \sum_i \frac{e^{-m_a r_a r_a - m_{r_s} r_s r_s} x\, Si\, \Delta x \Delta y}{2 r^2} \qquad (15)$$

where the distance to a volume element is just

$$r = \sqrt{x^2 + y^2} \tag{16}$$

The path length through the air is given by

$$r_a = \frac{rh}{y} \qquad (q > q_b) \tag{17}$$

and

$$r_a = \frac{rX}{x} \qquad (q < q_b) \tag{18}$$

where $2_b = \tan^{-1}(h/X)$ defines the angle from the horizontal to the juncture of the well floor and wall. The path length through the soil for all values of $2$ is then just

$$r_s = r - r_a \tag{19}$$

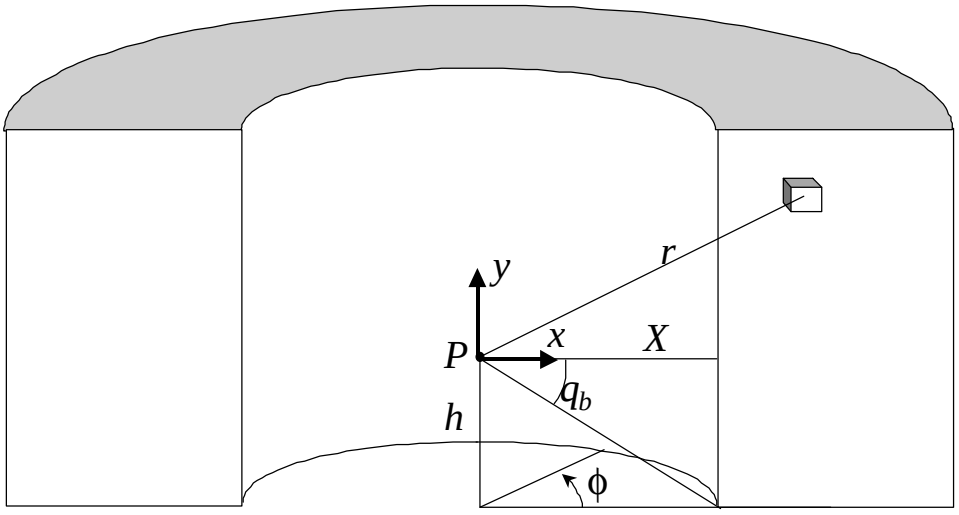


**Figure 7.** Cross section of a cylindrical well geometry.

Figure 8 shows the results of the calculations for the center of the well 1 m above the floor ($h$ = 1 m) for wall distances (radii) of 1, 2, 3, 5, and 10 m, as a function of wall heights from 1 to 5 m. Two sets of curves are shown, one for a representative low energy of 100 keV and the other for a representative high energy of 1000 keV. In place of reporting the actual fluence at these energies, the fluence relative to that for the standard values for these energies at 1 m above flat ground and a uniform distribution in the soil, designated as $\Phi_{1m}$, are given. These relative fluence values thus represent the degree of overestimate one would make in performing a measurement in such a well and reporting a concentration based on a detector calibration for the standard flat ground geometry, assuming there is no significant difference due to the angular dependence in the detector response.

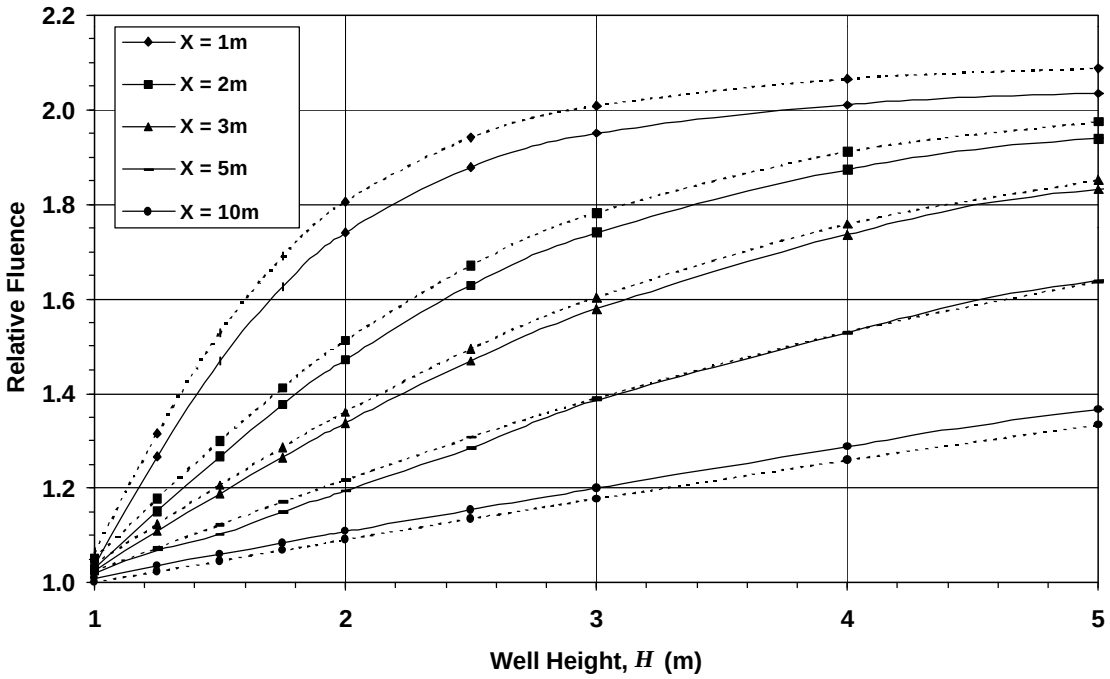


**Figure 8.** Relative fluence results from numerical integration for well geometry for a detector 1 m above the floor (dashed line - 100 keV; solid line - 1000 keV).

For wells 1 m in height (the same height as the detector), the relative fluence is just a few percent above unity. This is consistent with the findings for soil mounds below the plane of the detector. In essence, surrounding the detector with a ring at the same height maintains the $2\pi$ geometry of the normal flat ground half space. The fluence is only slightly higher because the outer regions of the ground have been folded up to a wall which then results in less air attenuation as compared to the outlying areas for flat ground.

Also, the fluence for an extremely narrow and deep well ($X$ = 1 m, $H$ = 5 m) is somewhat higher than twice that of flat ground. This results from the fact that it is nearly a $4\pi$ geometry (double that of flat ground) and, on average, there is a smaller air path length for the photons.

It is of some interest to examine the contributions from the floor and wall of the well to the total fluence measured. Again, the fluence relative to that for the standard values for these energies at 1 m above flat ground and a uniform distribution in the soil are given. Figure 9 shows the relative contribution from the floor as a function of wall distance, X. The wall contribution would thus be the total relative amount as given in Figure 8 minus this quantity. For example, for X = 1 m at 100 keV, the relative contribution from the floor is 0.3 using Figure 9. In Figure 8, the total for a well height of 2 m is 1.8, meaning about one sixth of the fluence comes from the floor as compared to five sixths from the wall for this case.

The results for either the 100 keV or 1000 keV in Figures 8 and 9 are not very different, despite the large range in energy. This is consistent with the behavior of the fluence data exhibited in Figure 1, that is, the solid angle effect dominates and the air attenuation effect is a second order effect. Hence, the relative fluence scales according to the well dimensions with relative insensitivity to energy.

Trench Geometry

For the generalized case of a trench with non-vertical walls, we refer to Figure 10 where $X_b$ is the half-width of the trench at its base (distance to the wall base from the center point), $H$ is the vertical trench height, and $\omega$ is the slope angle of the trench wall with respect to the horizontal.

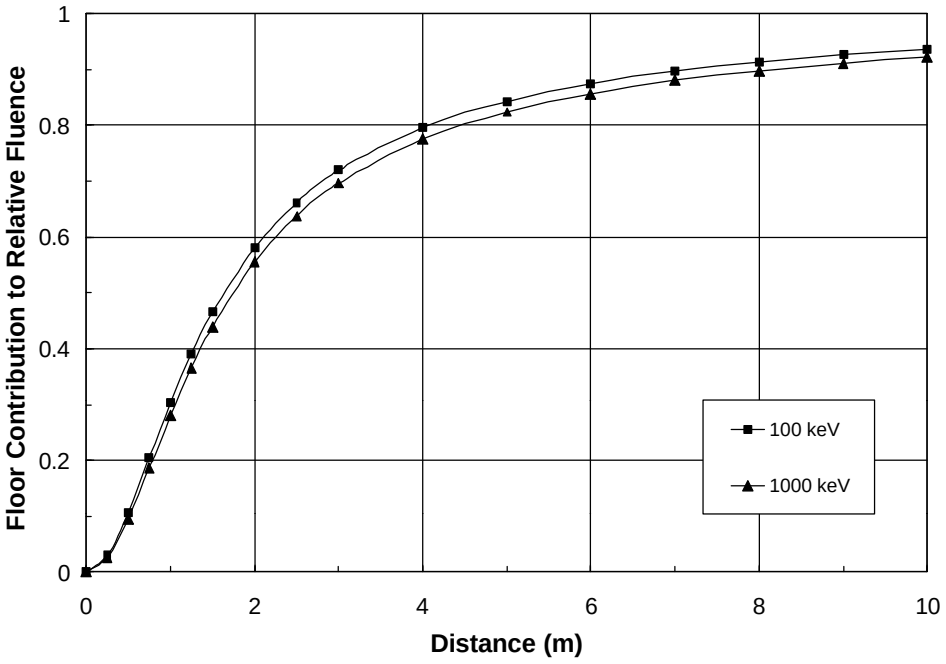


**Figure 9.** Relative contribution to fluence from floor of well.

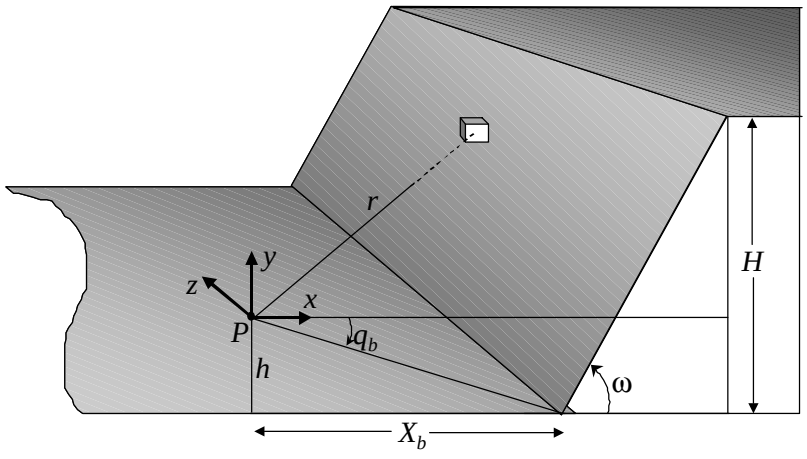


**Figure 10.** Generalized trench geometry (half view) with sloped wall.

Given the origin of the coordinate system at point P, the distance to any volume element can be expressed in rectangular coordinates as

$$r = \sqrt{x^2 + y^2 + z^2} \tag{20}$$

For $2 < 2_b$ the air and soil path lengths are given by the same equations for a cylindrical well (Equations 17-19), i.e., the photon path is through the floor using the above expression for $r$. Also, $2_b = f(z)$, specifically

$$q_b = \tan^{-1}\left(\frac{h}{\sqrt{X_b^{\,2} + z^2}}\right) \tag{21}$$

In the plane defined by $z = 0$, the path length through the soil for $2 > 2_b$ is given by

$$r_{s_0} = \frac{\left[x - X_b - \frac{(h + y)}{\tan w}\right] \sin w}{\sin[w - \tan^{-1}(y/x)]} \tag{22}$$

and for $z \neq 0$, the soil path length is scaled as

$$r_s = \frac{r}{\sqrt{x^2 + y^2}}\, r_{s_0} \tag{23}$$

The air path, for all values of $2$ and $z$, is then just

$$r_a = r - r_s \tag{24}$$

Figures 11 and 12 present the results of calculations at the center of a trench for cases of vertical (ω = 90°) and sloped walls (ω = 26.565°, i.e. tan ω = 0.5 or a 1:2 wall slope) for a detector height of 1 m above the trench floor. Given the rather small differences between energies as exhibited by the results for the well geometry, calculations were performed only for 1000 keV. Again, the fluence is expressed as relative to that for 1 m above flat ground.

As in the case of the well geometry, trenches at the same height as the detector result in a fluence that is only slightly higher than that of flat ground. Also, the fluence for narrow deep trenches ($X$ = 0.5 m vertical wall) will approach double that for flat ground.

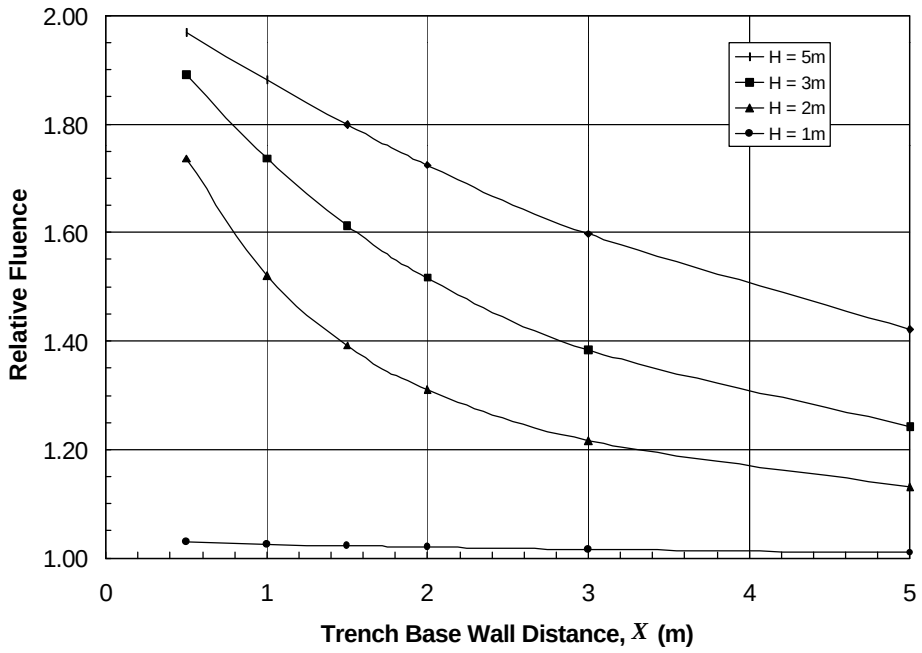


**Figure 11.** Relative fluence results from numerical integration for vertical wall trench geometry at 1000 keV for a detector 1 m above the floor.

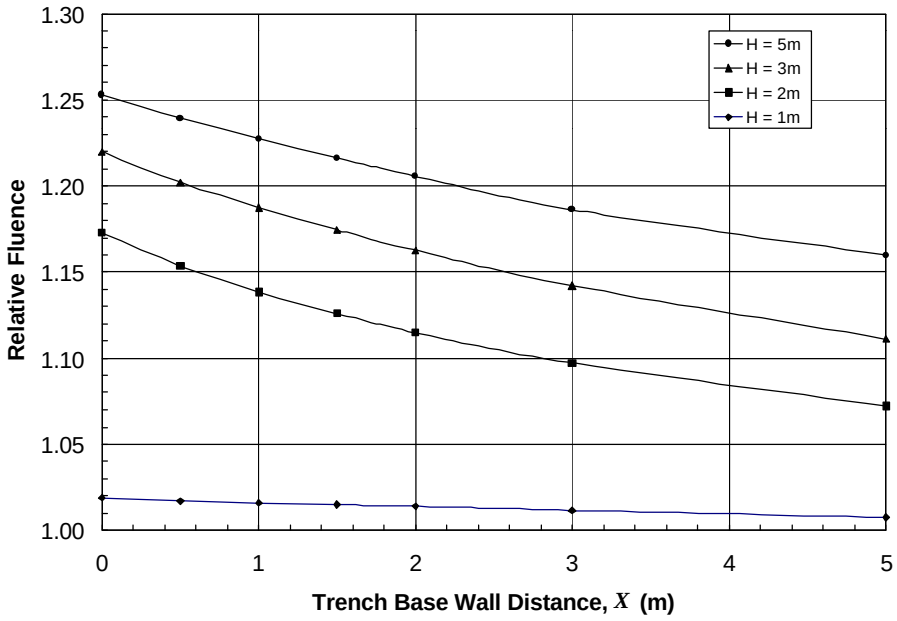


**Figure 12.** Relative fluence results from numerical integration for sloped (2:1) wall trench geometry at 1000 keV for a detector 1 m above the floor.

Analogous to Figure 9, Figure 13 presents the relative fluence contribution at 1000 keV from the floor of the trench as a function of distance to the wall. For any given wall distance, the trench geometry has a higher fraction of fluence from the floor area as compared to the well geometry since the floor extends to infinity in the *z* direction. For instance, at $X$ = 1 m, the relative fluence contribution is about 0.5 as compared to about 0.3 for the well geometry. Also, the effect of sloping the wall decreases the fluence contribution from the wall for the same $H$ value. This can be understood intuitively as the solid angle subtended by the wall becomes smaller as it slopes away from point *P*.

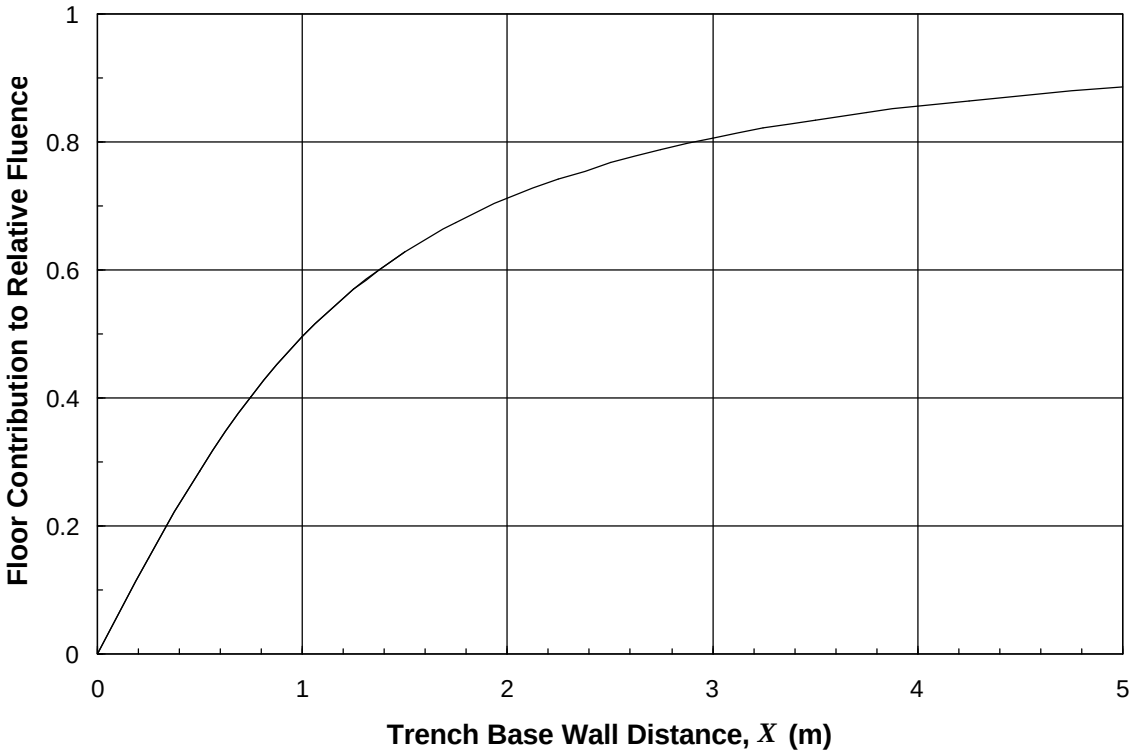


**Figure 13.** Contribution to fluence from the floor of a trench for a detector 1 m above the floor at 1000 keV.

## HORIZON ANGLE PARAMETERIZATION

From Equations 5 and 11, we can see that the solid angle can be expressed purely as a function of the horizon angle, $2_c$, for well and trench geometries. Since the fluence can be expected to vary according to the solid angle subtended by the soil, we can take the results of the calculations for the well and trench geometries and express them as a function of the single parameter, $2_c$, rather than the two dimensions *X* and *H*.

Figures 14 (100 keV) and 15 (1000 keV) shows the relative fluence for the well geometry as a function of $2_c$ as individual points along with two continuous curve fits for various *X* and *H* combinations (same data set as used in Figure 8). The upper curve (broken line) represents the relative fluence that is predicted on the basis of the solid angle (no air attenuation), that is,

$$\frac{\Phi_\Omega}{\Phi_{1m}} = \frac{\Omega S_0}{4p m_r r \Phi_{1m}} \tag{25}$$

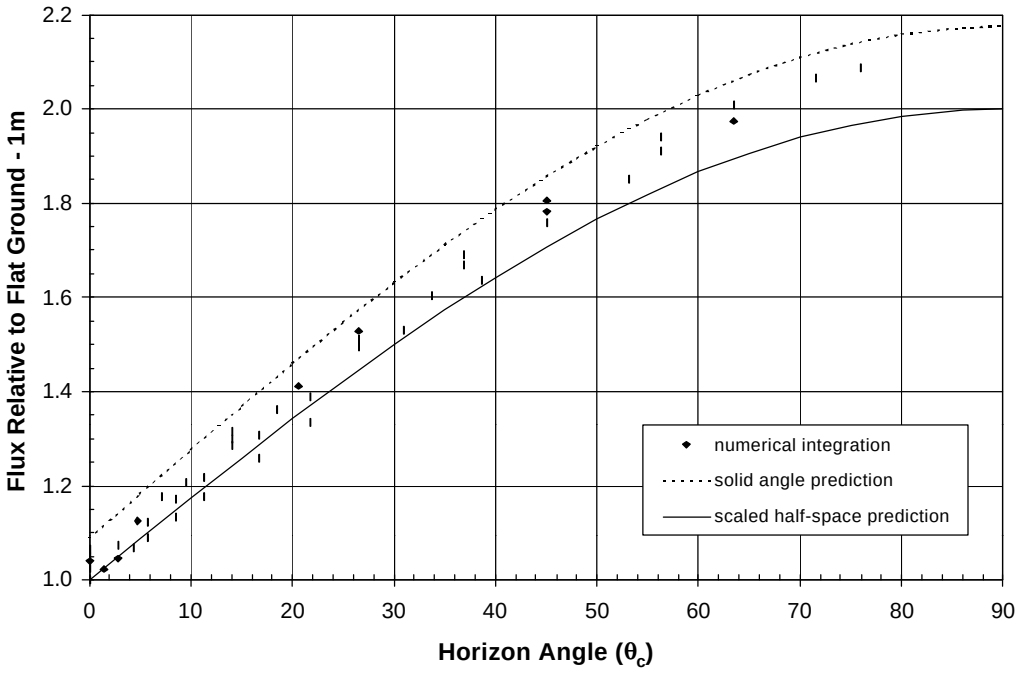


**Figure 14.** Relative fluence for the well geometry as a function of the horizon angle, $2_c$ for 100 keV.

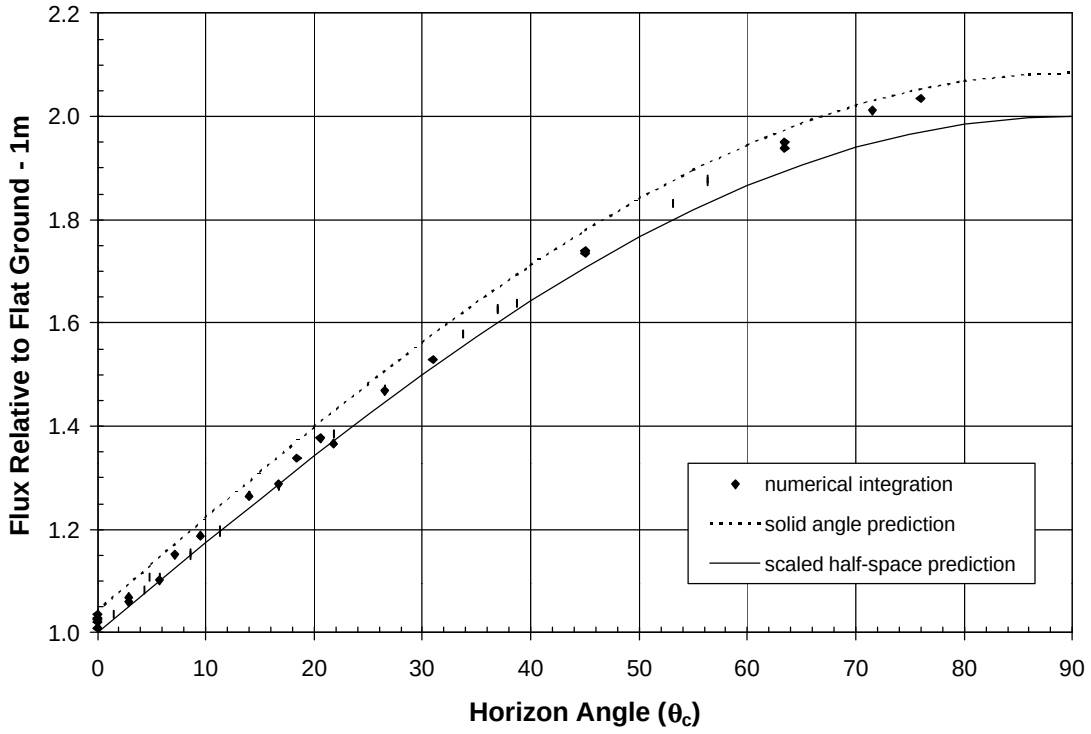


**Figure 15.** Relative fluence for the well geometry as a function of $\theta_c$ for 1000 keV.

The lower curve (solid line) represents the fluence as calculated for normal flat ground scaled according to the increase in solid angle above that of a half space. This curve thus includes the effects of air attenuation and assumes that the effect scales proportionately with the increase in the solid angle. This is expressed as

$$\frac{\Phi_s}{\Phi_{1m}} = \frac{\Omega}{2p} \tag{26}$$

The two curves more or less bound the numerical integration values with the range being about ± 10% for 100 keV and about ± 5% for 1000 keV. The differences seen for two or more data points at the same horizon angle value are due to the effects of air attenuation. A higher wall further away that subtends the same solid angle as a smaller wall close up will have a lower fluence due to an longer average air path length for the fluence.

The values of the fluence from the numerical integration are always less than the simple solid angle prediction. This is due to air attenuation effects that are neglected in the solid angle prediction. In contrast, the calculated fluence values tend to be higher than the scaled half space prediction. This is due to an overcompensation, on average, for the effects of air attenuation using the scaled half-space prediction.

Figures 16 and 17 present the analogous data for the case of the trench geometry. Here a limited set of values were computed at 100 keV (Figure 16) using the same range in $X$ and $H$ as before. In addition to the data generated for a height of 1 m above the floor, fluence values were calculated for a number of $X$ and $H$ combinations, where $h$ = 0.3 m. Deviations of the numerical integration values from the two curves tend to be a few percent for 100 keV. For 1000 keV, the values are in very good agreement with the curves, given the estimated 1% error in the calculation. Overall, the figures demonstrate the relative insensitivity of the fluence to energy, wall base distance, wall slope, wall height and detector height when simply using $2_c$ as the basis for computing fluence.

## OFF-CENTER POSITIONS IN TRENCHES

For a small well geometry, a measurement in the center is a logical position to obtain an average concentration. However, excavation work to support environmental remediation is more likely to produce trench-like geometries. In practice, it will then be necessary to perform measurements not only at regular intervals along the length of the trench ($z$ direction), but also across the width of the trench ($x$ direction). Given the fairly good accuracy with which fluence can be predicted using the single parameter $2_c$, the variation with $x$ can be shown via solid angle

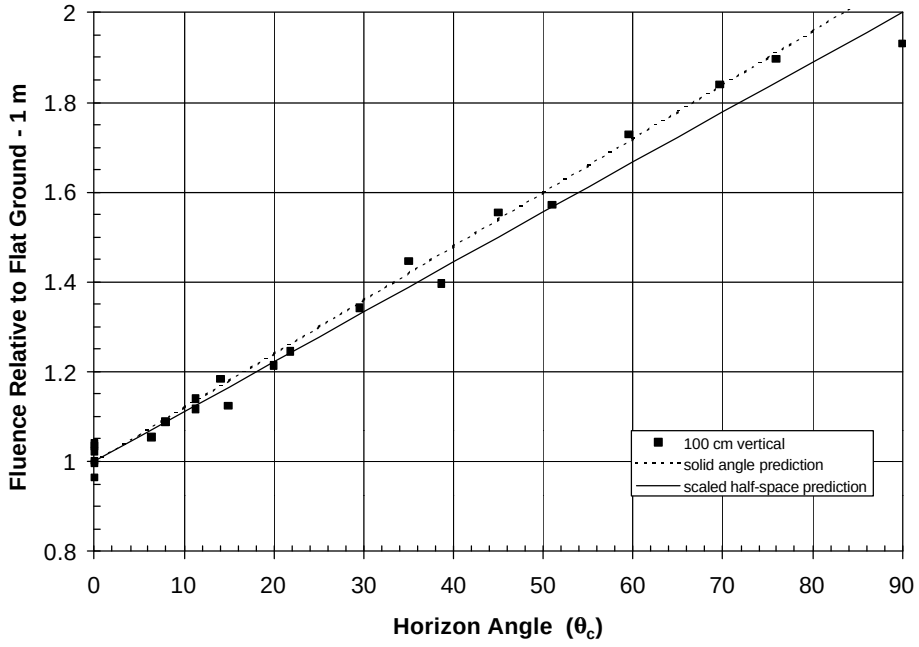


**Figure 16.** Relative fluence for the trench geometry as a function of $2_c$ for 100 keV.

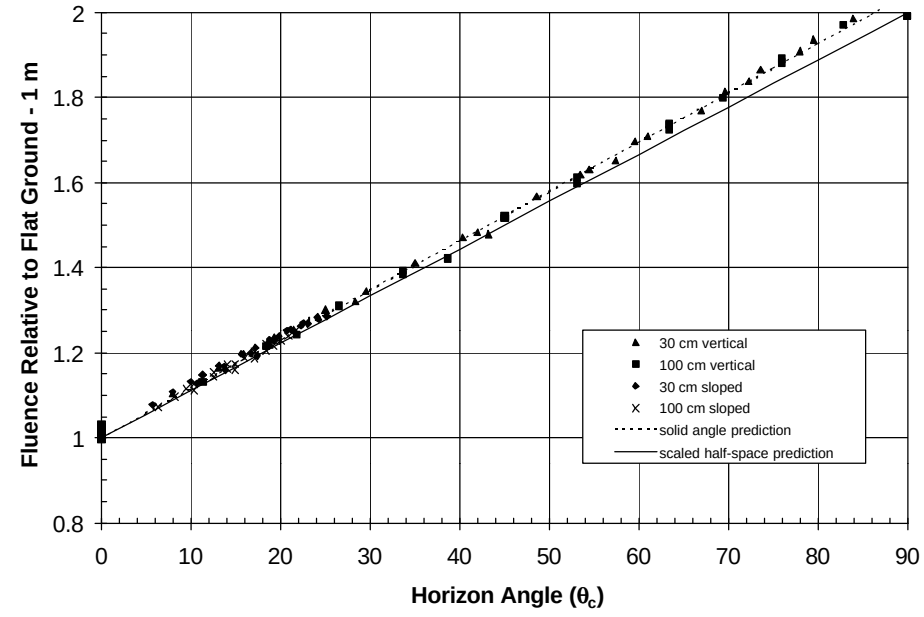


**Figure 17.** Relative fluence for the trench geometry as a function of $2_c$ for 1000 keV.

computations by considering two half trenches, i.e., two single walls at different distances. (In some cases, a single wall may be present which effectively reduces the geometry to a half trench.) By symmetry, Equations 10 and 11 can be rewritten as the sum of two components so that the total solid angle is given by

$$\Omega_t = 2p + 2\tan^{-1}\left(\frac{H-h}{X-x}\right) + 2\tan^{-1}\left(\frac{H-h}{X+x}\right) = 2(p + q_{c1} + q_{c2}) \qquad (27)$$

where $x$ is the distance off center and $2_{c1}$ and $2_{c2}$ are the horizon angles for the two walls.

Figure 18 graphs this function for a detector height of 1 m for two different wall heights (2 and 5 m) and four different trench half-widths (1, 2, 3, and 5 m) as a function of the offset distance from the trench centerline. In the case of the 5 m wall height, the fluence is relatively insensitive to the position in the trench for half-widths of up to 5 m. In the case of the 2 m wall height, most of the increase in the solid angle is seen to occur when distances are within 1 m or so from one of the walls. Thus, in practice, exact positioning of a detector is not necessary to obtain an accurate reading as long as one is not very close to the wall. Intuitively, this can be understood as the angle $2_c$ changes rapidly as one gets close to the wall face. In the limit, the solid angle subtended by the wall becomes $2\pi$ on contact and with a quarter-space contribution from the trench floor of $\pi$ (half the normal flat ground contribution), the total solid angle would be $3\pi$, not including any contribution from the more distant opposite wall.

# DETECTOR CONSIDERATIONS

## ANGULAR DISTRIBUTION OF FLUENCE

The complete calibration of a detector for *in situ* spectrometry entails the evaluation of its response to photon fluence over all angles of incidence. For cylindrical-shaped detectors mounted with their axis of symmetry perpendicular to the ground, variations in the response

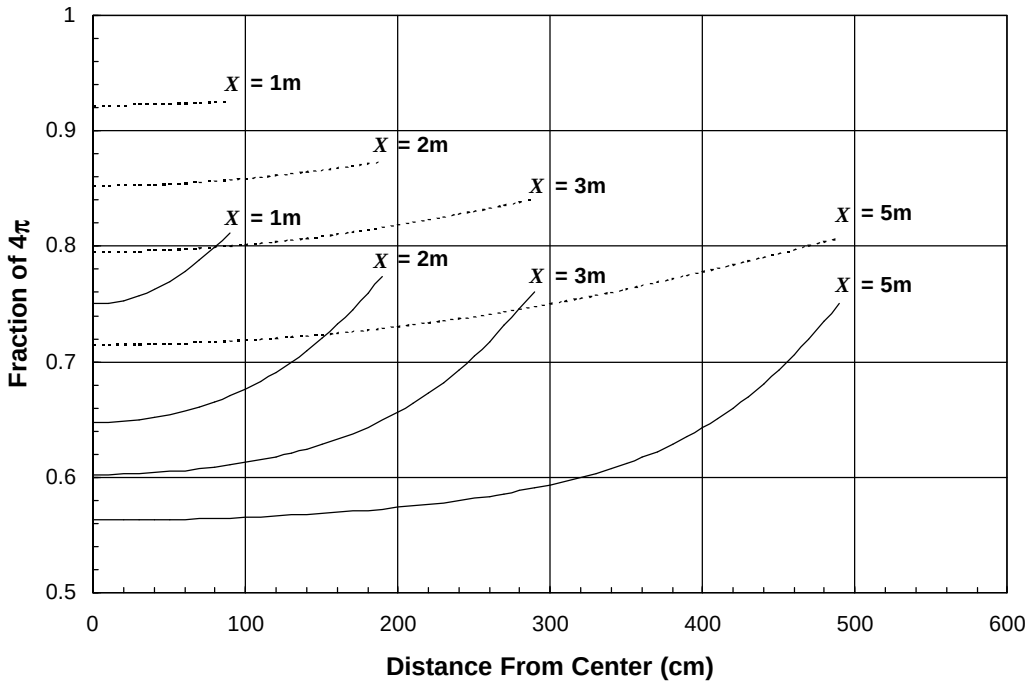


**Figure 18.** Fraction of full 4π solid angle as a function of distance from trench center for $H$ = 2 m (solid line) and $H$ = 5 m (dashed line).

about the azimuth angle $N$ are generally negligible. However, this is generally not the case for the zenith angle, $2$ (which in this case we measure from the vertical to the soil interface.) For this reason, an angular correction factor is computed which weights the relative response of the detector normalized to the detector face, $R(2)$, with fluence distribution. For a flat ground geometry, there is no dependence of $\Phi$ on $N$, so that the angular correction factor (counts measured in the given geometry relative to counts at normal incidence) is computed by

$$N_f / N_o = \frac{\int_0^{p/2} R(q')\Phi(q')dq'}{\int_0^{p/2} \Phi(q')dq'} \qquad (28)$$

For the case of flat ground, the distribution of Φ with respect to $2N$ is fairly insensitive to the photon energy for uniform source distributions in the soil. This is evidenced by the two distributions shown in Figure 9 that show little difference between 100 and 1000 keV as a function of *X*. In view of the domination of the solid angle effect, we would expect Φ to vary as sin $2N$. Indeed, even for the case of flat ground geometry where there is long air path lengths at large angles to the soil interface, Φ follows sin $2N$ to within a 3% or less.

Figure 19 shows data from an experimental determination of R at four different energies for one particular germanium (Ge) co-axial detector that is mounted to a small hand-held Dewar. This Ge crystal, in this case, had a length/diameter ratio of 0.8 which leads to the general characteristic fall-off in response for sidewall (90°) photon incidence. The very sharp fall-off for angles greater than 150° results from shielding by the Dewar. However, as evidenced by the sin $2N$ function, the weighting is large at angles near sidewall incidence.

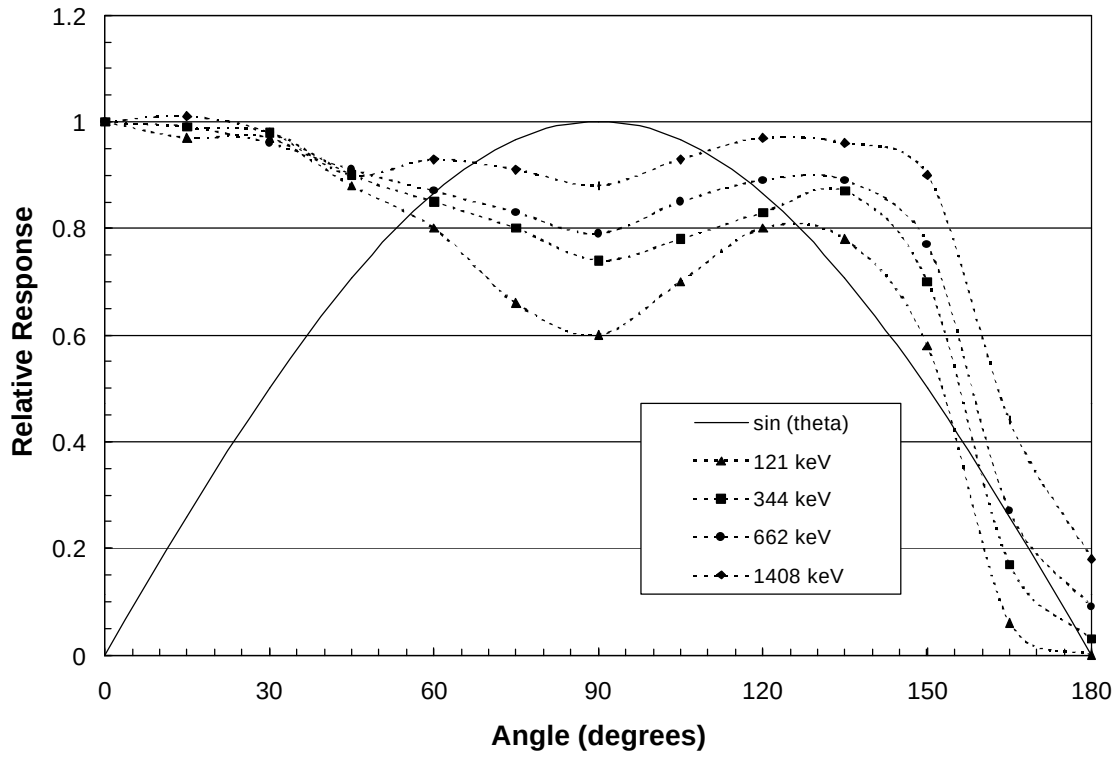


**Figure 19.** Example of angular response for a Ge detector as compared to relative solid angle (sin function).

In principle, the limits of integration in Equation 28 can be adjusted to compute an angular correction factor for any geometry with symmetry about $N$, such a cylindrical well. Table 1 lists the evaluations for three different geometries using the data in Figure 19. Going from the flat ground case to the extreme of a full $4\pi$ space shows that the detector response would only change by 11% at the lowest energy and just 2% at the highest. The $0^\circ$ to $120^\circ$ case would be representative of wells that are not too deep with respect to their width at the top, e.g., a 1:2 wall slope. Here, the difference between the angular correction factors from those of flat ground are reduced to 6% at the lowest energy and 0% at the highest.

In the case of trenches, the distribution of $\Phi$ will vary with both $2N$ and $N$. However, in this case, the difference in the angular correction factor from that of flat ground would become even less than that of the well geometry since a larger fraction of $\Phi$ will originate from the floor of the trench.

The relative insensitivity of the angular correction factor has important practical implications. If this quantity does not change significantly for a detector from that of flat ground, then a single correction factor that is representative of the likely geometries to be encountered can be used. This obviates the need to make individual evaluations for each source geometry. It must be pointed out, however, that the response of the detector across the range of incident angles needs to be checked to insure this. If they are to be used in measurements, particular attention must be made to low energies where most variation will occur.

**TABLE 1**

EXAMPLE ANGULAR CORRECTION FACTORS
FOR THREE DIFFERENT GEOMETRIES

| | Energy (keV) | | | |
|---|---|---|---|---|
| Geometry | 121 | 344 | 662 | 1408 |
| Flat ground | 0.81 | 0.86 | 0.89 | 0.93 |
| 0 to $120^\circ$ | 0.76 | 0.83 | 0.87 | 0.93 |
| $4\pi$ | 0.72 | 0.80 | 0.84 | 0.91 |

## PRACTICAL APPLICATION IN THE FIELD

Below-grade applications of *in situ* spectrometry present additional challenges with respect to personnel and equipment handling as compared to standard measurements on flat ground. Despite the added complexity of having to determine the geometry correction factor, below grade measurements have one advantage, namely, there is better definition of the soil volume being measured. That is to say, the field of view of the detector is restricted to the soil inside the well or trench. Contributions from distant sources are screened out by the very nature of the source geometry and the soil shielding properties. After excavation of contaminated soil, it is the remaining soil in the walls and floor of the cavity that require measurement to certify if cleanup criteria have been met.

Interestingly, the well geometry is like that of a standard re-entrant (Marinelli) beaker counting geometry that is commonly used for soil samples for laboratory-based gamma-ray spectrometry systems. The detector is surrounded on its sides and front face with the source containing material. In some sense, the well with the detector at its center represents an ideal geometry where there is a near equal contribution from the surrounding soil volume elements. A reasonably good "true" average is obtained of the radionuclide concentration, notwithstanding variations that may occur with depth into the wall or floor of the well.

The trench geometry, while not as confined as that of a well, can be treated in a linear fashion by making measurements at regular intervals along the length of the trench. Defining a trench as an individual survey unit would be a reasonable approach and, in this way, a reasonable average may be had.

To better define potential areas of remaining contamination (wall vs. floor, for example), detector collimation can be employed. In this case, calibration must be performed over the viewing area of the detector with the collimator in place. In lieu of this, deconvolution techniques can be applied. These have been demonstrated to perform well for applications over flat ground (Reginatto et al. 1997) and, in principle, should work equally well for a geometry such as a trench.

The situation may arise where there is known or suspected dichotomous source distribution in the surrounding soil, for instance, uranium contamination at the bottom of a well and some natural background concentration in the walls. In this situation, the fluence contribution and the concentration of the background source would have to be determined and the following formula applied

$$c_c = \frac{c_m - \left(\Phi_b / \Phi_t\right) c_b}{1 - \left(\Phi_b / \Phi_t\right)} \qquad (29)$$

where $\chi_c$ is the total concentration in the contaminated volume, $\chi_m$ is the effective average concentration measured by the detector, $\chi_b$ and $\Phi_b$ are concentrations in, and the fluence from the background volume, and $\Phi_t$ is the total fluence.

# CONCLUSIONS

The application of *in situ* spectrometry to the case of non-flat terrain is not precluded by the complexity of the source geometry. One can perform the necessary calculations to derive the fluence per unit source activity for any geometry. Since the detector response to fluence is independently determined, the measured fluence can be converted to concentration in the surrounding media.

In the case of soil mounds or similar projections below the plane of the detector, there is minimal change in the fluence from that of flat ground for uniform source distributions. Since below terrain geometries are more confined than that of a flat ground geometry, the effect of air attenuation is diminished to the point where basic solid angle estimates should suffice in most cases for determining the fluence at a measurement point.

For compliance purposes, an overestimate of the concentration is more desirable than an underestimate. In applying a calibration factor, a measured count rate is converted to fluence rate by dividing by the efficiency of the detector, and the resulting measured fluence rate is in turn converted to concentration by dividing by the predicted fluence rate per unit concentration. This means that scaling the predicted fluence that is derived for flat ground geometry by the ratio of solid angles (equation 26) would generally provide a conservative estimate of concentration. Alternatively, one can apply the flat ground calibration factors to some geometry, *a*, and then scale the measured concentration according to the ratio of solid angles to give the concentration in geometry, *a* , i.e.

$$c_a = \frac{2p}{\Omega_a} c_m \qquad (30)$$

The application of simple solid angle scaling must take into account the angular response of the detector. The angular correction factor needs to evaluated for various geometries to ensure that errors would be acceptable. Where they are not, specific calibration factors must then be applied to the measurement geometry. Particular care must be exercised for low energies.

Overall, it appears that the use of simple solid angle corrections would not introduce more than a few percent error in measurements of concentrations. Since the specification of a geometry in terms of the precise dimensions is difficult to determine in practice, acceptance of a few percent error is not unreasonable. Where rough characterization is to be done, this is well within acceptable limits on error. For certification or final status measurements, this degree of error may also be acceptable depending upon data quality objectives.

# REFERENCES


Beck, H. L., J. DeCampo, and C. Gogolak
*In Situ* Ge(Li) and NaI(Tl) Gamma-Ray Spectrometry
U. S. Atomic Energy Commission Report HASL-258, New York, NY (1972)

International Commission on Radiation Units and Measurements (ICRU)
Gamma-Ray Spectrometry in the Environment
ICRU Report 53, Bethesda, Maryland (1994)

Laedermann, J.-P., F. Byrde, and C. Murith
*In-Situ* Gamma-ray Spectrometry: the Influence of Topography on the Accuracy of Activity Determinations
J. Environ. Radioactivity 38:1-16 (1998)

Miller, K. M. and H. L. Beck
Indoor Gamma and Cosmic Ray Exposure Rate Measurements using a Ge Spectrometer and Pressurized Ionisation Chamber
Radiation Protection Dosimetry 7:185-190 (1984)

Miller, K. M., M. Reginatto, P. Shebell, G. A. Klemic, and C. V. Gogolak
Spectrometric Techniques for Measurement of Radioactive Contamination in Buildings
Proceedings of Air & Waste Management Association's 90th Annual Meeting, Pittsburgh, PA (1997)

Reginatto, M., P. Shebell, and K. M. Miller
ISD97, a Computer Program to Analyze Data From a Series of *In Situ* Measurements on a Grid and Identify Potential Localized Areas of Elevated Activity
USDOE Report EML-590 (1997)

USAEC, United States Atomic Energy Commission
T. Rockwell, III (Editor)
*Reactor Shielding Design Manual*
McGraw-Hill, New York (1956)

# APPENDIX A

The following are listings of the BASIC programs used in the numerical integrations of fluence for the cases of a cylindrical well, vertical wall trench and sloped wall trench source geometries. Note that variable names are in some places different from the notation used in this report. Also, the + y direction is down and the origin is set at the detector height.

For the most complicated case involving the sloped wall trench, the running time for a single case is several hours using a 200 MHz Pentium PC.

```
10 REM "FLUXPIT" MODIFIED JULY 1, 1998
20 REM THIS PROGRAM USES NUMERICAL INTEGRATION IN DOUBLE PRECISION
30 REM TO COMPUTE FLUX IN A CYLINDICAL PIT WITH UNIFORM
CONCENTRATION
35 REM INTEGRATION IS CARRIED ONLY TO 100 CM DEPTH AND 1 METER BEYOND
RADIUS
40 INPUT "ENTER PIT WALL DEPTH(cm) WHERE 0 IS DET. HEIGHT AND + IS DOWN: ",
MH:
50 INPUT "ENTER RADIUS OF PIT - I.E. DISTANCE TO PIT WALL(cm): ", X1:
70 INPUT "ENTER MU/RHO FOR AIR: ", XAIR: MUAIR = .0012 * XAIR
80 INPUT "ENTER MU/RHO FOR SOIL: ", XSOIL: MUSOIL = 1.6 * XSOIL

100 FOR X = 0 TO X1: PRINT X, FLX#
110 FOR Y = 100 TO 200
120 R = SQR((X + .5) * (X + .5) + (Y + .5) * (Y + .5))
124 AX = 100 * R / (Y + .5)
126 SX = R - AX
140 GOSUB 800
150 NEXT Y
160 NEXT X
170 FLOOR# = FLX#

200 FOR X = X1 TO (X1 + 100): PRINT X, FLX#
210 FOR Y = MH TO 99
220 R = SQR((X + .5) * (X + .5) + (Y + .5) * (Y + .5))
224 AX = X1 * R / (X + .5)
226 SX = R - AX
240 GOSUB 800
250 NEXT Y
260 NEXT X
270 WALL# = FLX# - FLOOR#

300 FOR X = X1 TO (X1 + 100): PRINT X, FLX#
310 FOR Y = 100 TO 200
315 YLIM = 100 * X / X1
320 R = SQR((X + .5) * (X + .5) + (Y + .5) * (Y + .5))
```

```
322 IF (Y + .5) > YLIM THEN AX = 100 * R / (Y + .5): GOTO 326
324 AX = X1 * R / (X + .5)
326 SX = R - AX
340 GOSUB 800
350 NEXT Y
360 NEXT X
370 CORNER# = FLX# - WALL# - FLOOR#

500 PRINT
505 PRINT "TOTAL FLUX = ", FLX#
510 PRINT "FLOOR FLUX FRACTION = ", FLOOR# / FLX#
520 PRINT "WALL FLUX FRACTION = ", WALL# / FLX#
530 PRINT "CORNER FLUX FRACTION = ", CORNER# / FLX#
600 GOTO 999

800
810 FLX# = FLX# + (EXP(-MUAIR * AX) * EXP(-MUSOIL * SX) * 1.6 * (X + .5) / (2 * R *
R))
820 RETURN

999 END
```

```
10 REM "FLUXTRENCH VERSION 2" MODIFIED JUN 1, 1998
20 REM THIS PROGRAM USES NUMERICAL INTEGRATION IN DOUBLE PRECISON MODE
30 REM TO COMPUTE FLUX FOR A RECTANGULAR TRENCH WITH UNIFORM CONCENTRATION
35 REM INTEGRATION IS CARRIED ONLY TO 100 CM DEPTH AND 30 M LENGTH
40 INPUT "ENTER DISTANCE TO WALL (CM)): ", X1
50 INPUT "ENTER WALL HEIGHT IN CM(WHERE 0 IS DETECTOR HEIGHT AND + IS DOWN): ", MH:
60 INPUT "ENTER DETECTOR HEIGHT ABOVE FLOOR: ", DH
70 INPUT "ENTER MU/RHO FOR AIR: ", XAIR: MUAIR = .0012 * XAIR
80 INPUT "ENTER MU/RHO FOR SOIL: ", XSOIL: MUSOIL = 1.6 * XSOIL

100 FOR X = 0 TO (X1 - 1)
110 FOR Y = DH TO DH + 100
115 FOR Z = 0 TO 3000
120 R = SQR((X + .5) * (X + .5) + (Y + .5) * (Y + .5) + (Z + .5) * (Z + .5))
124 AX = DH * R / (Y + .5)
126 SX = R - AX
140 GOSUB 800
145 NEXT Z
150 NEXT Y
160 PRINT X, FLX#: NEXT X
170 FLOOR# = FLX#

200 FOR X = X1 TO (X1 + 100)
210 FOR Y = MH TO DH - 1
215 FOR Z = 0 TO 3000
220 R = SQR((X + .5) * (X + .5) + (Y + .5) * (Y + .5) + (Z + .5) * (Z + .5))
224 AX = X1 * R / (X + .5)
226 SX = R - AX
240 GOSUB 800
245 NEXT Z
250 NEXT Y
260 PRINT X, FLX#: NEXT X
270 WALL# = FLX# - FLOOR#
```

```
300 FOR X = X1 TO (X1 + 100)
305 IF X1 = 0 THEN YLIM = DH + 101: GOTO 310
306 YLIM = DH * X / X1
310 FOR Y = DH TO DH + 100
312 FOR Z = 0 TO 3000
320 R = SQR((X + .5) * (X + .5) + (Y + .5) * (Y + .5) + (Z + .5) * (Z + .5))
322 IF (Y + .5) > YLIM THEN AX = DH * R / (Y + .5): GOTO 326
324 AX = X1 * R / (X + .5)
326 SX = R - AX
340 GOSUB 800
345 NEXT Z
350 NEXT Y
360 PRINT X, FLX#: NEXT X
370 CORNER# = FLX# - WALL# - FLOOR#

500 PRINT
505 PRINT "TOTAL FLUX = ", FLX#
510 PRINT "FLOOR FRACTION = ", FLOOR# / FLX#
520 PRINT "WALL FRACTION = ", WALL# / FLX#
530 PRINT "CORNER FRACTION = ", CORNER# / FLX#
600 GOTO 999



800
810 FLX# = FLX# + ((EXP(-MUAIR * AX) * EXP(-MUSOIL * SX) * 1.6) / (4 * 3.14159 * R *
R))
820 RETURN

999 END
```

```
10 REM "FLUXTRAP" MODIFIED APR. 8, 1998
20 REM THIS PROGRAM USES NUMERICAL INTEGRATION IN DOUBLE PRECISON MODE
30 REM TO COMPUTE FLUX FOR A SLOPED WALL TRENCH WITH UNIFORM CONCENTRATION
35 REM INTEGRATION IS CARRIED ONLY TO 100 CM DEPTH AND 30 M LENGTH
40 INPUT "ENTER DISTANCE TO WALL BASE (CM)): ", X1
50 INPUT "ENTER WALL HEIGHT IN CM(WHERE 0 IS DETECTOR HEIGHT AND + IS DOWN): ", MH:
55 INPUT "ENTER DETECTOR HEIGHT ABOVE FLOOR: ", DH
60 INPUT "ENTER SLOPE ANGLE OF WALL (DEGREES FROM HORIZONTAL): ", THETA: SLP = 3.141592654# * THETA / 180
65 X2 = X1 + CINT((DH - MH) / TAN(SLP)): PRINT " TOP OF WALL (X2) DISTANCE = ", X2
70 INPUT "ENTER MU/RHO FOR AIR: ", XAIR: MUAIR = .0012 * XAIR
80 INPUT "ENTER MU/RHO FOR SOIL: ", XSOIL: MUSOIL = 1.6 * XSOIL

100 FOR X = 0 TO (X1 - 1)
110 FOR Y = DH TO DH + 100
115 FOR Z = 0 TO 3000
120 R = SQR((X + .5) * (X + .5) + (Y + .5) * (Y + .5) + (Z + .5) * (Z + .5))
124 AX = DH * R / (Y + .5)
126 SX = R - AX
140 GOSUB 800
145 NEXT Z
150 NEXT Y
160 PRINT X, FLX#: NEXT X
170 FLOOR# = FLX#

200 FOR X = X1 TO (X2 + 100)
202 YTOP = DH - ((X + .5 - X1) * TAN(SLP))
204 IF YTOP < MH THEN YTOP = MH
210 FOR Y = YTOP TO DH - 1
212 R0 = SQR((X + .5) * (X + .5) + (Y + .5) * (Y + .5))
215 FOR Z = 0 TO 3000
220 R = SQR((X + .5) * (X + .5) + (Y + .5) * (Y + .5) + (Z + .5) * (Z + .5))
```

```
222 S0N = ((X + .5 - X1 - (DH - (Y + .5)) / TAN(SLP))) * SIN(SLP)
224 S0D = SIN(SLP + ATN((Y + .5) / (X + .5)))
226 SX = (R / R0) * (S0N / S0D)
228 AX = R - SX
240 GOSUB 800
245 NEXT Z
250 NEXT Y
260 PRINT X, FLX#: NEXT X
270 WALL# = FLX# - FLOOR#


300 FOR X = X1 TO (X2 + 100)
305 IF X1 = 0 THEN YLIM = DH + 101: GOTO 310
306 YLIM = DH * X / X1
310 FOR Y = DH TO DH + 100
312 FOR Z = 0 TO 3000
320 R = SQR((X + .5) * (X + .5) + (Y + .5) * (Y + .5) + (Z + .5) * (Z + .5))
322 IF (Y + .5) > YLIM THEN AX = DH * R / (Y + .5): SX = R - AX: GOTO 340
328 R0 = SQR((X + .5) * (X + .5) + (Y + .5) * (Y + .5))
330 S0N = ((X + .5 - X1 - (DH - (Y + .5)) / TAN(SLP))) * SIN(SLP)
332 S0D = SIN(SLP + ATN((Y + .5) / (X + .5)))
334 SX = (R / R0) * (S0N / S0D)
336 AX = R - SX
340 GOSUB 800
345 NEXT Z
350 NEXT Y
360 PRINT X, FLX#: NEXT X
370 CORNER# = FLX# - WALL# - FLOOR#

500 PRINT
505 PRINT "TOTAL FLUX = ", FLX#
510 PRINT "FLOOR FRACTION = ", FLOOR# / FLX#
520 PRINT "WALL FRACTION = ", WALL# / FLX#
530 PRINT "CORNER FRACTION = ", CORNER# / FLX#
600 GOTO 999
```

```
800
810 FLX# = FLX# + ((EXP(-MUAIR * AX) * EXP(-MUSOIL * SX) * 1.6) / (4 * 3.14159 * R *
R))
820 RETURN

999 END
```